Articles

^{11}B Nutation NMR Study of Powdered Borosilicates

Ae Ja Woo*, Duk-Young Han†, and Kyung Hwa Yang‡

*Department of Science Education, Ewha Womans University, Seoul 120-750, Korea
†Korea Basic Science Institute, Seoul 136-701, Korea
‡Department of Chemistry, Ewha Womans University, Seoul 120-750, Korea
Received August 25, 1997

In this work, we applied the 1D ^{11}B nutation NMR method for the analysis of the local structural environments in powdered borosilicates (SiO_2-B_2O_3). Spin dynamics during a rf irradiation for spin I=3/2 was analytically calculated with a density matrix formalism. Spectral simulation programs were written in MATLAB on a PC. Two borosilicates prepared by the sol-gel process at different stabilization temperature were used for the 1D ^{11}B nutation NMR experiment. The ^{11}B NMR parameters, quadrupole coupling constants (e^2qQ/h) and asymmetry parameters (η), for each borosilicate were extracted from the nonlinear least-squares fitting. The effects of heat treatments on the local structures of boron sites in borosilicates were discussed.

Introduction

Solid-state NMR spectroscopy has been widely used for the structural investigations in inorganic solids having quadrupole nuclei ($I \geq 1$) such as ^2H, ^{11}B, ^{23}Na, ^{27}Al, ^{55}Mn, etc. The quadrupolar interaction parameters, quadrupole coupling constant (e^2qQ/h) and asymmetry parameter (η), give informations about magnitude and shape of the electric field gradient at the quadrupolar nuclei site, respectively. So these values are sensitive to the local symmetry and give the direct structural information. Various NMR methods are available for the study of quadrupolar interaction by the analysis of central transition lineshape and spinning sideband. With MAS (magic angle spinning),[1,2] VAS (variable angle spinning),[3] DAS (dynamic angle spinning),[4,5] and DOR (double rotation)[6] NMR methods, it has been possible to reduce the second order quadrupolar line broadening partially by averaging the inherent anisotropic quadrupolar interaction.

2D Nutation NMR for especially half-integer spin system has been proven to be a valuable method for the study of quadrupolar interaction. When $\omega_Q(=3e^2qQ/8I(2I-1)/h)$ and ω_{rf} represent the quadrupolar interaction strength and the rf pulse strength, respectively, nutation NMR spectrum can be distinguished into three cases; (1) when $\omega_Q \gg \omega_{rf}$, the nutation spectrum illustrates a single absorption signal at $(I+1/2)\omega_{rf}$ nutation frequency, (2) when $\omega_Q \ll \omega_{rf}$, the nutation spectrum also illustrates a single absorption signal at ω_{rf} nutation frequency, and (3) when $\omega_Q \approx \omega_{rf}$, the nutation spectrum becomes a function of ω_Q and ω_{rf} and shows characteristic first order quadrupolar powder pattern. For a static powdered sample, conventional high field wideline spectrum shows that the central transition is perturbed by quadrupolar interaction combined with chemical shielding. So if we have more than one nuclear site in the sample, overlapping powder patterns are really hard to resolve. 2D nutation NMR can resolve the overlapping powder patterns: it is possible to separate informations on each of two dimensions. The F2 dimension yields the conventional wideline spectrum. The F1 dimension yields the characteristic nutation spectrum. In addition, it is possible to determine the quadrupolar interaction parameters, e^2qQ/h and η, in the 1D nutation NMR spectrum from the relative intensity of the central transition signal according to the rf pulse length t_1.

Spin dynamics during a rf excitation pulse such as x, -x, rotary-echo, or two opposite pulse has been calculated for spin I=3/2,[7-13] 5/2,[12-16] 7/2,[12,13] and 9/2[12,13,17] system. 1D and 2D nutation NMR spectroscopy has been experimentally used for the measurement of quadrupolar interaction parameters in $^{27}Al_2O_3$ and $NH_4{}^{27}Al(SO_4)_2 \cdot 12H_2O$,[14,15] the quantitative determination of 4-coordinated framework and 6-coordinated non-framework ^{27}Al sites in zeolite Y,[18-20] the investigation of nucleation and growth behavior of lithium disilicate,[21] the structural phase transition of $^{87}RbCaF_3$,[22] and the measurement of bond length in amorphous solids.[23]

Herein, we will show the effects of heat treatments on the local structures of boron sites in borosilicates by using 1D ^{11}B nutation NMR method. For this, we are trying to establish our theoretical basis with numerical simulation for nutation NMR method of spin I=3/2 system.

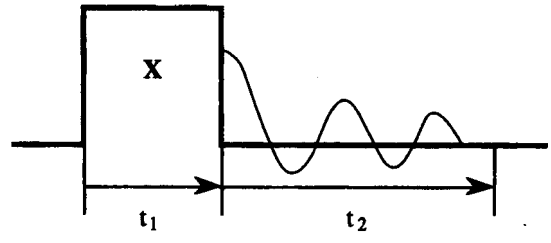

Scheme 1

*To whom correspondence should be addressed.
† Present address: Radiation Safety Research Group, Korea Electric Power Research Institute, Taejon 305-380, Korea

Theory

Scheme 1 shows a graphical description for the x-nutation NMR pulse sequence.

With *rf* pulse on resonance, the Hamiltonian in the rotating frame during t_1 is given by

$$H_{on} = H_{rf} + H_Q^{(1)} = -\omega_{rf} I_x + \frac{1}{4}\omega_Q a_o(\theta, \phi)\left(\frac{I_z^2 - I(I+1)}{3}\right) \quad (1)$$

where $\omega_Q = \dfrac{3e^2qQ}{8I(2I-1)\hbar}$

$$a_o(\theta, \phi) = (3\cos^2\theta - 1 + \eta\sin^2\theta\cos 2\phi).$$

H_{rf} and $H_Q^{(1)}$ represent the coupling of the spin with the *rf* magnetic field and the first order quadrupolar interaction, respectively. θ and ϕ are Euler angles needed to orient the principal axis of electric field gradient tensor with respect to the applied magnetic field. If the rf pulse is much stronger than quadrupolar interaction, $H_Q^{(1)}$ in Eqn. (1) can be neglected, which is a prerequisite for ordinary FT-NMR.

For spin I=3/2 system, matrix representation for H_{on} is given like

$$H_{on} = \begin{bmatrix} \frac{\omega_Q a_o}{4} & -\frac{\sqrt{3}\omega_{rf}}{2} & 0 & 0 \\ -\frac{\sqrt{3}\,\omega_{rf}}{2} & -\frac{\omega_Q a_o}{4} & -\omega_{rf} & 0 \\ 0 & -\omega_{rf} & -\frac{\omega_Q a_o}{4} & -\frac{\sqrt{3}\omega_{rf}}{2} \\ 0 & 0 & -\frac{\sqrt{3}\omega_{rf}}{2} & \frac{\omega_Q a_o}{4} \end{bmatrix} \quad (2)$$

Unitary matrix (T) diagonalizing Hamiltonian can be found by solving secular equation like $H_{on}\Psi_i = \lambda_i\Psi_i$ or $\mathrm{Det}(H_{on} + \lambda \mathrm{II}) = 0$. The result is as follows:

$$T = \frac{1}{\sqrt{2}}\begin{bmatrix} c1 & s1 & -s2 & c2 \\ -s1 & c1 & c2 & s2 \\ -s1 & c1 & -c2 & -s2 \\ c1 & s1 & s2 & -c2 \end{bmatrix} \text{ and}$$

$$T^+ H_{on} T = \begin{bmatrix} \lambda_1 & 0 & 0 & 0 \\ 0 & \lambda_2 & 0 & 0 \\ 0 & 0 & \lambda_3 & 0 \\ 0 & 0 & 0 & \lambda_4 \end{bmatrix} \quad (3)$$

where $c1 = \cos\frac{\theta_1}{2}$, $c2 = \cos\frac{\theta_2}{2}$, $s1 = \sin\frac{\theta_1}{2}$, $s2 = \sin\frac{\theta_2}{2}$,

$$\cos\theta_1 = \frac{1+2\alpha_Q}{2\sqrt{1+\alpha_Q+\alpha_Q^2}},\ \cos\theta_2 = \frac{1-2\alpha_q}{2\sqrt{1-\alpha_Q+\alpha_Q^2}},$$

$$\sin\theta_1 = \frac{\sqrt{3}}{2\sqrt{1+\alpha_Q+\alpha_Q^2}},\ \sin\theta_2 + \frac{\sqrt{3}}{2\sqrt{1-\alpha_Q+\alpha_Q^2}}$$

$$\lambda_1 = \omega_{rf}(-\frac{1}{2} + \sqrt{1+\alpha_Q+\alpha_Q^2}),\ \lambda_3 = \omega_{rf}(\frac{1}{2} + \sqrt{1-\alpha_Q+\alpha_Q^2}),$$

$$\lambda_2 = \omega_{rf}(-\frac{1}{2} + \sqrt{1+\alpha_Q+\alpha_Q^2}),\ \lambda_4 = \omega_{rf}(\frac{1}{2} - \sqrt{1-\alpha_Q+\alpha_Q^2}),$$

and where $\alpha_Q = \dfrac{1}{4}\dfrac{\omega_Q a_o(\theta, \phi)}{\omega_{rf}}$.

The dynamics of spin system can be obtained by solving the Liouville-von Neumann equation. The evolution of density matrix during t_1 on the rotating frame is given by

$$\begin{aligned}\rho(t_1,\ t_2=0)_{ij} &= \{\exp(-iH_{on}t_1)\,\rho(0)\exp(iH_{on}t_1)\}_{ij} \\ &= \{T\exp(-iT^+H_{on}Tt_1)T^+\,\rho(0)\,T\exp(iT^+H_{on}Tt_1)\,T^+\}_{ij} \\ &= \sum_{k,l}\{T_{ik}T_{jl}\exp\{-i(\lambda_k-\lambda_1)t_1\}(T^+\rho(0)T)_{kl}\}\end{aligned}$$

Thus, $\rho(t_1,\ t_2)_{ij} = \rho(t_1,\ t_2=0)_{ij}\ \exp\{-i(\omega_i-\omega_j)t_2\}$

$$= \exp\{-i(\omega_i-\omega_j)t_2\}\sum_{k,l}\{T_{ik}T_{jl}\exp\{-i(\lambda_k-\lambda_1)t_1\}(T^+\rho(0)T)_{kl}\}. \quad (4)$$

where the equilibrium density matrix $\rho(0)$ corresponds to I_z. The central transition (i, j=1/2, −1/2) coherence is supposed to be detected, because only the central transition coherence excited by a rf irradiation survives during the deadtime. The density matrix at the end of a rf pulse associated with the central transition coherence is described by

$$\begin{aligned}\rho(t_1, t_2=0)_{1/2,-1/2} = \\ &(1+\cos\theta_1+\cos\theta_2+\cos\theta_1\cos\theta_2-3\sin\theta_1\sin\theta_2)\sin(\lambda_2-\lambda_3)t_1 \\ &+(1-\cos\theta_1+\cos\theta_2-\cos\theta_1\cos\theta_2+3\sin\theta_1\sin\theta_2)\sin(\lambda_1-\lambda_3)t_1 \\ &+(1+\cos\theta_1-\cos\theta_2-\cos\theta_1\cos\theta_2+3\sin\theta_1\sin\theta_2)\sin(\lambda_2-\lambda_4)t_1 \\ &+(1-\cos\theta_1-\cos\theta_2+\cos\theta_1\cos\theta_2-3\sin\theta_1\sin\theta_2)\sin(\lambda_1-\lambda_4)t_1 \quad (5)\end{aligned}$$

where $(\lambda_2-\lambda_3)$, $(\lambda_1-\lambda_3)$, $(\lambda_2-\lambda_4)$, and $(\lambda_2-\lambda_4)$ represent four nutation frequencies resulted from one triple quantum (23) and three single quantum transition coherences (13, 24, and 14). The transitions are indicated in the energy level diagram in Scheme 2.

The central transition FID during t_1 can be calculated by

$$S(t_1,\ t_2=0)_{1/2,-1/2} = Tr\{\rho(t_1,\ t_2=0)(I_x+iI_y)\}_{1/2,-1/2} = i\rho_{-1/2,1/2}. \quad (6)$$

The expression results in only the imaginary components because the *rf* pulse along the x-direction is applied. But suppose we apply pulse along y-direction, the signal would appear along x in real experiment, then the signal detected would correspond to real sign. In addition, the central transition FID during t_2 is given by

$$S(t_1,\ t_2)_{1/2,-1/2} = S(t_1,\ t_2=0)_{1/2,-1/2}\exp(-i\Omega t_2). \quad (7)$$

where the second order quadrupolar shift, $\Omega = \dfrac{3}{4\omega_0}\left[\dfrac{e^2qQ}{4h}\right]^2$ $(1-\cos^2\beta)(1-9\cos^2\beta)$ for η=0. FT in t_2 of Eq. (6) and double FT in t_2 and t_1 of Eq. (7) give 1D and 2D nutation NMR spectrum, respectively.

Experimental

Sample Preparation. Two borosilicate samples (SiO_2-

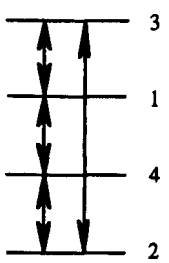

Scheme 2

B_2O_3) were prepared by the sol-gel process; mixing, aging, drying, and stabilization. More details are described in literature.[24] Sample labels BS150 and BS850 are based on the stabilization temperature 150 °C and 850 °C, respectively. According to Oldfield *et al.*,[25] borates and borosilicates show two kinds of local structures at boron sites, trigonal (BO_3) and tetrahedral (BO_4); the ^{11}B quadrupolar interaction is small in BO_4 (e^2qQ/h=0-0.8 MHz) and larger in BO_3 (e^2qQ/h=2.4-2.8 MHz).

Solid-State 1D ^{11}B Nutation NMR Spectroscopy. Solid-state 1D ^{11}B nutation NMR spectra were acquired on a Bruker MSL200 solid-state NMR spectrometer operating at 64.2 MHz. The sample was packed into 5 mm glass sample holder for a static wideline probe. The x-nutation NMR pulse sequence was used. The rf pulse length (t_1) was incremented in steps of 2 μs, typically from 1 to 99 μs. The rf pulse strength (ω_{rf}) was adjusted to ~36 kHz which corresponds to 180° pulse length of 14 μs by using an aqueous solution of boric acid. A relaxation delay of 10 s and a dead time of 10 μs were used. Each spectrum was obtained by summing 120 free induction decays (FID). Exponentially filtering of 1 kHz and zero filling of 1 K were applied. The relative intensity of the central transition signal was measured from the integration of Fourier-transformed and manually-phased spectrum. The ^{11}B chemical shift values are referenced to external trifluoride diethyletherate (BF_3Et_2O).

Simulations. No corrections for the rf field inhomogeniety, the relaxation effect, and the second-order quadrupolar interaction effect were made in the spectral simulations. In this work all simulations are done for static powdered samples with spin I=3/2 system. All spectra calculated from Equations. (6) and (7) are simulated by summing the four nutation frequencies for Euler angles θ and φ orientations over the range of 0 to 90° with sin(θ) weighting. Typically, we use a uniform step angle of 1° and the calculation takes about 5 minutes for a nutation spectrum (512 data size) and about 50 minutes for a 2D nutation spectrum (256×128 data size) on a PentiumPro PC. Simulation programs were written in MATLAB v5, a vector oriented programming language.

Results and Discussion

Figure 1 shows the calculated relative intensity of central transition signal in the 1D nutation spectrum versus the *rf* pulse length t_1 for several values of e^2qQ/h with η=0 at ω_{rf}= 50 kHz. It clearly illustrates that the precession frequency and amplitude of the relative signal intensity are dependent on the values of quadrupolar interaction parameters. In comparison with two extreme cases in the nutation theory, ω_Q (= $3e^2qQ/8I(2I-1)h$) $\gg \omega_{rf}$ and $\omega_Q \ll \omega_{rf}$, both magnetizations converge into sine curves; the magnetization of the former (e^2qQ/h=1000 kHz) precesses almost twice faster frequency and half smaller amplitude than that of the latter (e^2qQ/h=0). The qualitative understanding is as follows. For very weak quadrupolar interaction ($\omega_Q \ll \omega_{rf}$), all coherences including sideband coherences are flocked together so that the *rf* pulse strength satisfies the strong pulse condition. This situation should be similar to the case for solution sample. For very strong quadrupolar interaction ($\omega_Q \gg \omega_{rf}$), the central band coherence isolated from sideband coherences precesses much faster because the *rf* pulse can excite only the central coherence. In this case, the central band coherence can be treat-

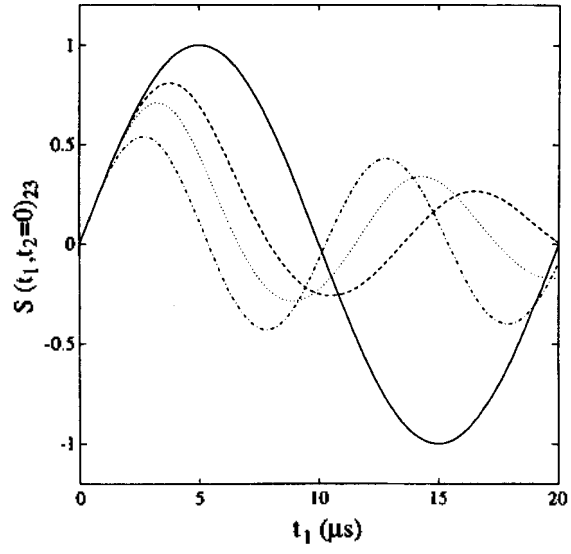

Figure 1. Calculated relative intensity of the central transition signal in the 1D nutation NMR versus the *rf* pulse length t_1. Parameters used in the calculation are as follows: ω_{rf}=50 kHz, η= 0, and e^2qQ/h=0 (—), 300 kHz (---) 500 kHz (···), and 1000 (—·—·—) kHz.

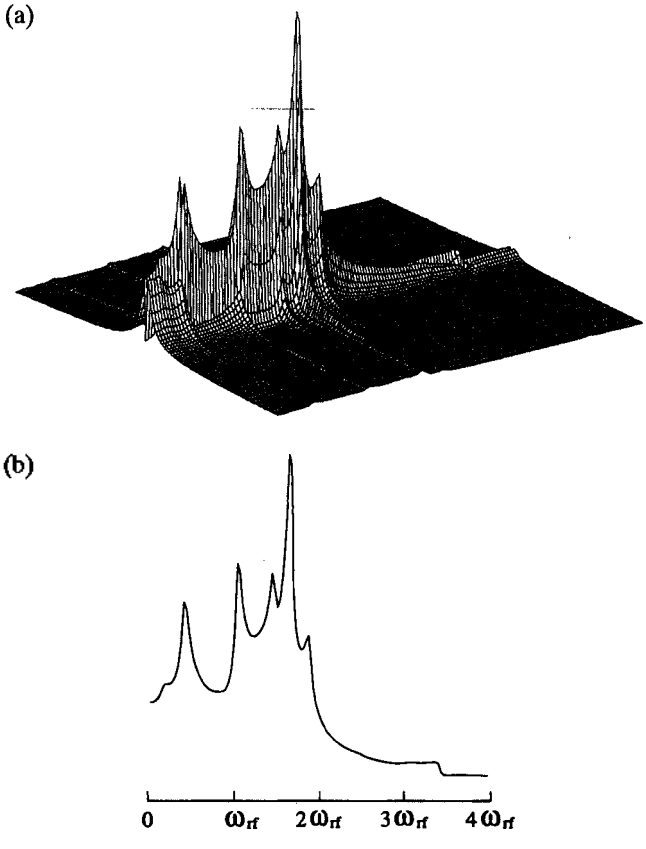

Figure 2. (a) Calculated 2D nutation NMR spectrum for spin I= 3/2 system and (b) the projection along the F1 dimension. Parameters used in the calculation are as follows: ω_{rf}=50 kHz, η= 0, and e^2qQ/h=300 kHz.

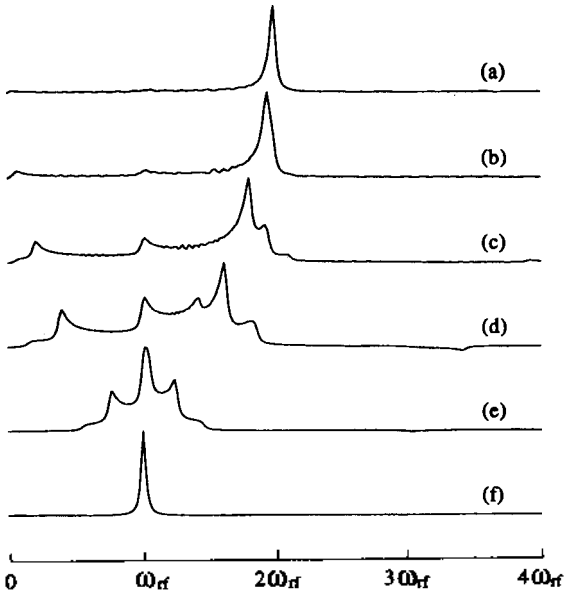

Figure 3. Calculated nutation NMR spectra for spin I=3/2 system. Parameters used in calculation are as follows: ω_{rf}=50 kHz, η=0, and e^2qQ/h=(a) 2000, (b) 1000 kHz, (c) 500 kHz, (d) 300 kHz, (e) 100 kHz, and (f) 0 kHz. The scale factors are (a) 0.30, (b) 0.18, (c) 0.12, (d) 0.10, (e) 0.19, and (f) 1.0.

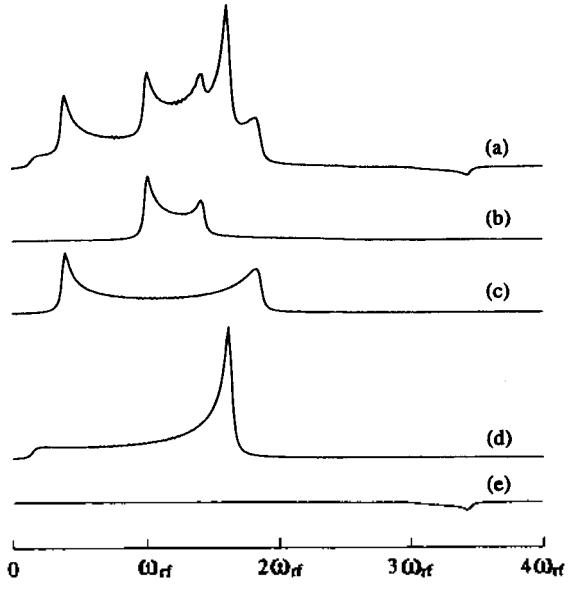

Figure 4. Calculated nutation NMR spectrum for spin I=3/2 system with the values of e^2qQ/h=300 kHz and η=0 at ω_{rf}=50 kHz. Four separated powder patterns calculated from each nutation frequency are shown in (a) total, (b) $(\lambda_1-\lambda_4)$, (c) $(\lambda_2-\lambda_4)$, (d) $(\lambda_1-\lambda_3)$, and (e) $(\lambda_2-\lambda_3)$.

ed as an isolated fictitious spin-1/2 operator.

Figure 2 shows a calculated 2D nutation spectrum and its projection along the F1 dimension for the value of e^2qQ/h= 300 kHz with η=0 at ω_{rf}=50 kHz. An important feature of 2D nutation NMR is the separation of informations on each of two dimensions. Projection along the F2 dimension represents conventional high field wideline spectrum. Projection along the F1 dimension especially for the intermediate case ($\omega_Q \approx \omega_{rf}$) represents a characteristic nutation spectrum resulted from only quadrupolar interaction parameters.

Figure 3 shows the calculated nutation NMR spectra for several values of e^2qQ/h with η=0 at ω_{rf}=50 kHz. These spectra correspond to the projections along the F1 dimension in 2D nutation spectra. The nutation spectra in two extreme cases, *i.e.* Figure 3(a) and (f), represent single absorption signals located at ω_{rf} and $2\omega_{rf}$, respectively. If the sample contains two nuclear sites with different strength of quadrupolar interaction, the F1 dimension yields two signals; one is located at ω_{rf} and the other at $2\omega_{rf}$. The intermediate nutation spectra, *i.e.* Figure 3(b) to (e), show rather characteristic nutation spectra. Shown in Figure 4 is a nutation spectrum and its four spectral components simulated from $(\lambda_2-\lambda_3)$ triple quantum and $(\lambda_1-\lambda_4)$, $(\lambda_2-\lambda_4)$, and $(\lambda_1-\lambda_3)$ single quantum transition coherences. The lineshapes of four powder patterns are quite different and the signal intensity from triple coherence is very weak relative to those from single coherences. Figure 5 shows the maximum and minimum nutation frequencies for the values of e^2qQ/h=0 to 1000 kHz with η=0 at ω_{rf}=50 kHz. The maximum and minimum nutation frequencies from $(\lambda_1-\lambda_3)$ and $(\lambda_2-\lambda_4)$ coherences are distributed between 0 and $2\omega_{rf}$. For $(\lambda_1-\lambda_4)$ and $(\lambda_2-\lambda_3)$ coherences, the minimum nutation frequencies are set to ω_{rf} and $3\omega_{rf}$, respectively, and the maximum values are largely dependent on the values of e^2qQ/h. Asterisks (*) on the

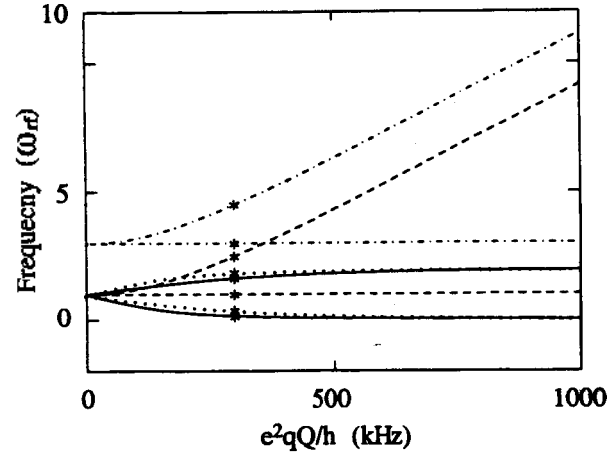

Figure 5. Maximum and Minimum nutation frequencies for spin I=3/2 system versus the values of e^2qQ/h=0 to 1000 kHz at η=0 and ω_{rf}=50 kHz. Four nutation transitions are represented as follows; $(\lambda_1-\lambda_4)$; ---, $(\lambda_2-\lambda_4)$; ..., $(\lambda_1-\lambda_3)$; —, and $(\lambda_2-\lambda_3)$; -·-·-. Asterisks (*) on the curves indicate the maximum and minimum values for e^2qQ/h=300 kHz and η=0 at ω_{rf}=50 kHz.

curves indicate the maximum and minimum values for e^2qQ/h=300 kHz, which are comparable with a nutation spectrum shown in Figure 4.

Shown in Figure 6 are the results of the nonlinear least-squares fit (−) of calculated signal intensities to the experimental signal intensities (•) of the 1D ^{11}B nutation NMR spectra for BS150 and BS850 borosilicates. The Levenberg-Marquardt nonlinear least-squares algorithm[26] was used. The fitted variables include the values of e^2qQ/h and η for two boron sites and their fraction in each borosilicate. The rf pulse strength (ω_{rf}) is fixed to 38 kHz instead of 36 kHz, ex-

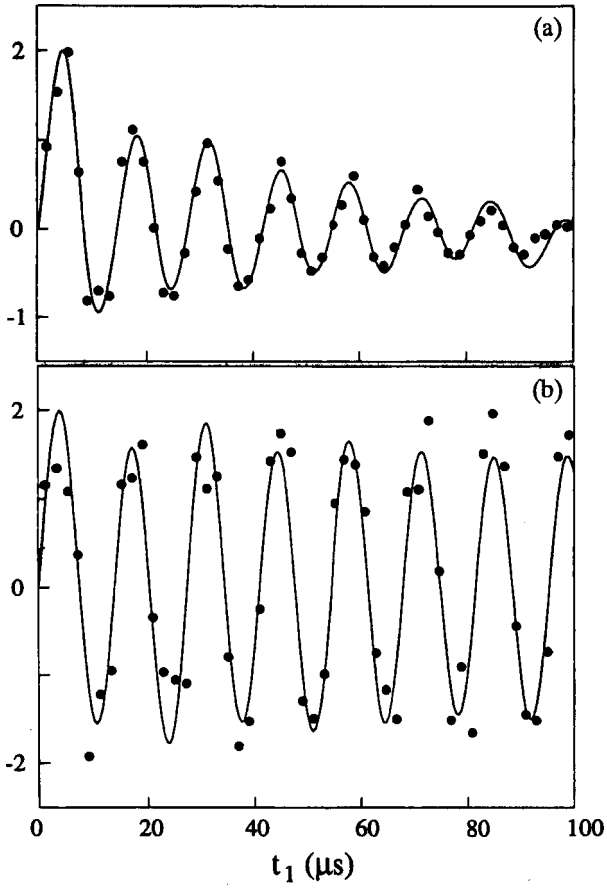

Figure 6. The nonlinear least-squares fit (—) of calculated signal intensities to the experimental signal intensities (●) of 1D ^{11}B nutation NMR spectra for (a) BS150 and (b) BS850 borosilicates. The fitted ^{11}B NMR parameters are listed in Table 1.

Table 1. The results of the nonlinear least-squares fitting for BS 150 and BS850 borosilicates

Sample Label	e^2qQ/h (MHz)	η	r	^{11}B Local Environment[c]
BS150	0.502 (1)	0.302 (3)	0.98 (9)[a]	Tetrahedral BO_4
BS850	2.46 (2)	0.045 (3)	1.00 (2)[b]	

[a] Fraction of BO_4 in boron sites. [b] Fraction of BO_3 in boron sites. [c] Predicted from the known values of e^2qQ/h and η.[25]

perimental value. The fitting results are listed in Table 1. BS150 and BS850 borosilicates are consisted of one kind of boron site, tetrahedral BO_4 and trigonal BO_3, respectively. An important feature is the observation of the effects of heat treatments on the local boron environment. As the stabilization temperature increases from 150 °C to 850 °C, the local structures of boron sites change from asymmetric ($\eta > 0$) tetrahedral BO_4 to symmetric ($\eta \approx 0$) trigonal BO_3. These results can be explained as follows. At 150 °C, because of the oxophilicity of boron atom in BO_3, it is more accessible to oxygen atom in remaining solvent, molecular water, and silanol group for the formation of tetrahedral BO_4. At 850 °C, the local structural changes from BO_4 to BO_3 is occurred by the dehydration.

2D nutation NMR method is useful for the separation of overlapping powder pattern having quadrupole nuclei at two dissimilar electric field gradients; one with a large quadrupolar interaction ($\omega_Q \gg \omega_{rf}$) and the other with a small quadrupolar interaction ($\omega_Q \ll \omega_{rf}$) with respect to the rf pulse strength. On the other hand, 1D nutation NMR is a valuable method for the determination of the values of e^2qQ/h and η from the analysis of the signal intensities. In this work, we need to obtain the values of e^2qQ/h and η and to explain the differences in the local boron environment for two kinds of borosilicate, thus 1D ^{11}B nutation NMR method was used.

Conclusions

We applied the 1D ^{11}B nutation NMR method for the determination of quadrupolar interaction parameters in powdered borosilicates. Four nutation frequencies were calculated by using a density matrix formalism. Based on the theoretical calculation, nutation spectra as a function of quadrupolar interaction parameters were simulated. There are two ways to acquire the quadrupolar interaction parameters by using a nutation NMR method. They can be extracted from (1) the projection along F1 dimension in the 2D nutation spectra for the intermediate case ($\omega_Q+\omega_{rf}$) and (2) the signal intensities in the 1D nutation spectra according to the rf pulse length (t_1). In this work, the second way was used to determine the quadrupolar interaction parameters in two borosilicates.

Acknowledgment. This work was supported by Faculty Research Grant (1996) funded by Ewha Womans University. Partial support by Korea Science and Engineering Foundation (971-0305-036-1) is also acknowledged. Korea Basic Science Institute is acknowledged for the use of the Bruker MSL200 solid-state NMR spectrometer.

References

1. Irwin, A. D.; Holmgren, J. S.; Jonas, J.; Non-Cryst, J. *Solids* **1988**, *101*, 249.
2. Haase, J.; Oldfield, E.; Schmitt, K. *Chem. Phys. Letters* **1992**, *193*, 274.
3. Ganapathy, S.; Shore, J.; Oldfield, E. *Chem. Phys. Letters* **1990**, *169*, 301.
4. Youngman, R. E.; Zwanziger, J. W. *J. Non-Cryst. Solids* **1994**, *168*, 293.
5. Mueller, K. T.; Sun, B. Q.; Chingas, G. C.; Zwanziger, J. W.; Terao, T.; Pines, A. *J. Magn. Reson.* **1990**, *86*, 470.
6. Wu, Y.; Sun, B. Q.; Pines, A. *J. Magn. Reson.* **1990**, *89*, 297.
7. Man, P. P. *J. Magn. Reson.* **1991**, *94*, 258.
8. Man, P. P. *Chem. Phys. Letters* **1990**, *168*, 227.
9. Man, P. P. *J. Magn. Reson.* **1988**, *77*, 148.
10. Janssen, R.; Veeman, W. S. *J. Chem. Soc., Faraday Trans.* **1988**, *84*, 3747.
11. Man, P. P. *J. Magn. Reson.* **1986**, *67*, 78.
12. Samoson, A.; Lippmaa, E. *J. Magn. Reson.* **1988**, *79*, 255.
13. Kentgens, A. P. M.; Lemmens, J. J. M.; Geurts, F. M. M.; Veeman, W. S. *J. Magn. Reson.* **1987**, *71*, 62.
14. Man, P. P. *Molecular Physics* **1993**, *78*, 307.
15. Van der Mijden, J. A. M.; Janssen, R.; Veeman, W. S. *Molecular Physics* **1990**, *69*, 53.

16. Geurts, F. M. M.; Kentgens, A. P. M.; Veeman, W. S. *J. Chem. Phys.* **1985**, *120*, 206.
17. Man, P. P.; Theveneau, H.; Papon, P. *J. Magn. Reson.* **1985**, *64*, 271.
18. Man, P. P.; Klinowski, J. *Chem. Phys. Letters* **1988**, *147*, 581.
19. Man, P. P.; Klinowski, J. *J. Chem. Soc., Chem. Commun.* **1988**, 1291.
20. Man, P. P.; Klinowski, J.; Trokiner, A.; Zanni, H.; Papon, P. *Chem. Phys. Letters* **1988**, *151*, 143.
21. Burkhard, D. J. M.; Nachtegaal, G. *J. Non-Cryst. Solids* **1997**, *209*, 299.
22. Trokiner, A.; Man, P. P.; Theveneau, H.; Papon, P. *Solid State Communications* **1985**, *55*, 929.
23. Horne, D.; Kendrick, R. D.; Yannoni, C. S. *J. Magn. Reson.* **1983**, *52*, 299.
24. Yang, K. H.; Woo, A. J. *Bull. Korean Chem. Soc.* **1996**, *17*, 696.
25. Turner, G. L.; Smith, K. A.; Kirkpatrick, R. J.; Oldfield, E. *J. Magn. Reson.* **1986**, *67*, 544.
26. Kim, A. J.; Butler, L. G. *Concepts in Magnetic Resonance* **1992**, *4*, 205.

Assay of Midazolam in Human Plasma by Gas-Liquid Chromatography with Nitrogen-Phosphorus Detection

Ho-Sang Shin*, Choon Pyo Hong, Yun-Suk Oh-Shin†, Bokyung Kang†, Kyungok Lee‡, and Kyupum Lee‡

Department of Environmental Education, Kongju National University, Kongju, Chungnam 314-701, Korea
†Korea Environment & Water Works Institute, Seoul 150-036, Korea
‡Seoul Clinical Laboratories, Seoul Medical Science Institute, Seoul 140-230, Korea
Received September 11, 1997

A sensitive and specific method is described for the determination of midazolam in human plasma. The drug was extracted from 1 mL of carbonate buffered plasma (pH 9.6) with 8 mL of diethyl ether. Famprofazone was used as internal standard. The organic phase was evaporated to dryness. The residue was dissolved in methanol for the direct analysis by gas chromatograph-nitrogen phosphorus detector system. In the concentration range of 1-5000 ng/mL, the calibration curve was linear. The coefficients of variation from the precision test were < 6% at the range of the concentration of 0.10-2.00 μg/mL and the detection limit for midazolam in 1 mL of plasma was 0.5 ng. This assay is more sensitive, selective, simple and rapid than earlier methods. Plasma midazolam concentrations were determined by this method after administration of midazolam.

Introduction

Midazolam [8-chloro-6-(2-fluorophenyl)-1-methyl-4H-imidazo(1,5-a)(1,4)-benzodiazepine] (Figure 1) is a benzodiazepine used as a premedicant and sedative in surgical and other procedures and for the induction of anaesthesia.

It is also used in the management of severe insomnia. Excessive drowsiness, sedation and ataxia are the most frequent adverse effects. Respiratory depression and hypotension have occurred after intravenous use for conscious sedation.[1] Although blood level studies have been described, currently available methods for determination of the drug in plasma are not suitable for pharmacokinetic studies in which single doses may be compared. Several methods based on different principles have been proposed for the determination of midazolam. For the determination of nanogram amounts of midazolam in biological fluids, the most commonly used methods employ high performance liquid chromatography (HPLC)[2-13] and gas chromatography (GC).[14-21] HPLC methods are not sensitive enough to determine the trace levels (down to 1 ng/mL) of midazolam present in human plasma. Several GC methods[14,18] measured plasma concentrations of midazolam by a single-step extraction procedure with a mixture of chloroform and ethylacetate (80 : 20),[14] or n-hexane-dichloromethane (70 : 30).[18] These solvents such as chloroform and dichloromethane are very toxic for human.

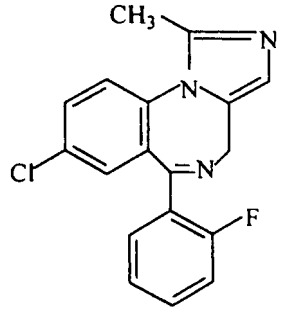

Figure 1. The structure of midazolam.

We propose a GC separation with NPD after a single extraction with diethyl ether for the selective and highly sen-